Preprint of book chapter 8 of "Photoelectrochemical Water Splitting: Issues and Perspectives," ed. H-J. Lewerenz and L.M. Peter, RSC Publishing, pp. 193-222 (2013). http://dx.doi.org/10.1039/9781849737739-00193

Chapter 8

The Group III-Nitride Material Class: from Preparation to Perspectives in Photoelectrocatalysis

Ramón Collazo[1] and Nikolaus Dietz[2]

[1]Department of Material Science & Engineering, NC State University, Raleigh, NC, 27606
[2]Department of Physics & Astronomy, Georgia State University, Atlanta, Georgia, 30303

Abstract:

In this chapter, the physical properties of group III-nitride compound semiconductors are reviewed in the context to act as semiconducting material in photoelectrocatalytic solar fuel structures. The band alignments in the InN-GaN-AlN-InN alloy system are summarized and discuss with respect to potential catalysts HOMO and LUMO states, providing efficient charge transfer in photoelectrochemical cell structures. The present status in group III-nitride materials fabrication and ternary alloy formation, stabilization and integration into envisioned materials structures is presented, together with challenges that have to be addressed to enable the full potential of group III-nitrides to contribute to high-efficient energy generation and utilization.

Table of Contents

8.1 Introduction

Renewable solar fuel generation either via photovoltaic (PV) cells or via photoelectrocatalytic solar fuel cells is expected to play a central role in the way energy is produced in the coming century to mitigate environmental problems associated with continued fossil fuels consumptions. Fuels generated by photoelectrocatalytic conversion may be hydrogen (H_2), methanol (CH_3OH), or other alkanes molecules that can store tremendous amounts of energy per mass unit. These solar fuels can release its energy in usable fashion upon reaction with oxygen (O_2) without producing environmental harmful byproducts. The formation of these envisioned solar fuels can be readily addressed through the development of compound semiconductor based electrolytic cells which have the advantage of producing the products at separate locations. Group III-nitrides compound semiconductors are ideally suited to drive such endergonic reactions with light, acting as the light absorbing units in hybrid photoelectrochemical (PEC) cells. The surfaces of these semiconductors have to be stabilized and modified with molecular or inorganic catalysts in order to catalyze specific desired reactions pathways. Research in this area will require materials of high-quality with well-defined tailored properties and reproducibility. In the following sections, we provide a brief review and present knowledge of the group III-nitrides compound semiconductors properties and the efforts in improving the structural and physical materials properties as well as the integration of dissimilar materials for the envisioned device functionalities.

8.1.1 Properties of the binaries InN, GaN, AlN and their ternaries

Binary group III-nitrides - e.g. AlN, GaN, InN, TlN, and their ternary and quaternary alloys - possess a number of attractive physical, optical, and electronic properties that allow the fabrication of novel materials and device structures, which are reviewed and a number of reviews over the last two decades.[1-11]

As depicted in Figure 8.1, the group III-nitrides can crystallize in a hexagonal wurtzite (wz) or in a cubic zinc blende (zb) crystal structure and span a wide range of bandgap energies, depending on composition. The most stable crystalline structure of the III-nitrides is the hexagonal wurtzite crystal structure, which are partially ionic solids due to large differences in the electronegativity of the group-III metal cations and nitrogen anions.[7] Due to the strong ionic III-N bonds, the unit cell of the III-nitrides is distorted from the ideal wurtzite unit cell, resulting in a large spontaneous polarization along the c-axis. The large differences in the ionic radii and bonding energies of the group III metal cations give rise to different lattice constants, bandgap energies, electron affinities, which challenges the epitaxial deposition of the III-nitrides and its alloys. At present, the lattice mismatch between the different III-nitride materials and commonly used substrates result in high dislocation densities, which impacts the optoelectronic and mechanical properties in the epilayers. Such dislocations also critically influence the surface morphology of heteroepitaxial III-nitride epilayers. Recently, due to advances in III-nitride native substrates, homoepitaxial and pseudomorphic heteroepitaxial films with lower dislocation densities have been achieved. The lower dislocation densities lead to an improved surface morphology, where the single crystalline surfaces are determined by surface energy minimization.

The bandgaps of three binaries InN, GaN, and AlN span from 0.7±0.05 eV[12,6,13] to 3.5±0.1 eV[7] through 6.1±0.1 eV[7], where the low bandgap value of InN is still undergoing revisions.[6]

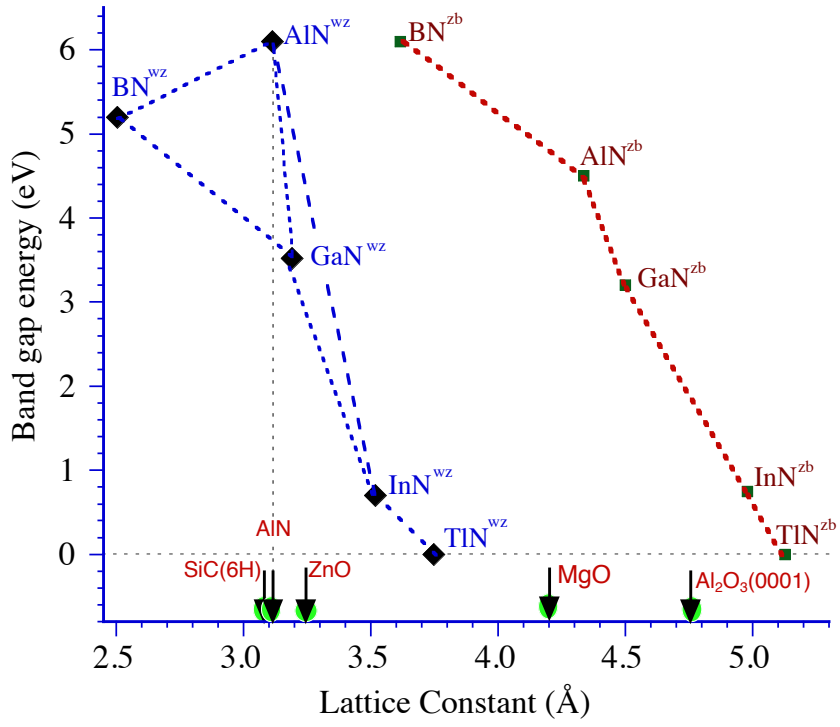

Figure 8.1: Lattice constants and bandgap energies for wurtzite (wz) and cubic zinc blende (zb) group III-nitride compound semiconductors, together with utilized substrates used in the growth of epilayers.

Recent assessments of the ternaries InGaN and InAlN alloy formation within a cluster expansion approach[14] substantiate the contribution of compositional instabilities to the wide spread bandgaps bowings of the indium-containing ternaries InGaN and InAlN,[15,16] affecting the short-range and long-range ordering of ternary alloys.

Table 8.1: Lattice parameter and bandgap values for group III-nitride alloys

Binary alloy	a (Å)	c (Å)	c/a ratio	u	Literature
wz - InN	3.517	5.685	1.616	1.616	Ref. [13]
wz - GaN	3.18940	5.18614	1.62606	0.3789	Ref. [17]
wz - AlN	3.1120	4.9808	1.60054	0.3869	Ref. [17]

Ternary bandgap values: $E_{g(A_xC_{1-x}N)} = E_{g(A)} \cdot x + E_{g(C)} \cdot (1-x) - b \cdot x \cdot (1-x)$

Ternary alloy	Bandgap $E_{g(A)}$ (eV)	Bandgap $E_{g(C)}$ (eV)	Bowing parameter b	Literature / Remarks
$In_xGa_{1-x}N$	0.70 ± 0.05	3.52 ± 0.1	1.6 ± 0.2	b= 1.65±0.07 Ref. [18] b= 1.36 Ref. [19]
$Al_xGa_{1-x}N$	6.10 ± 0.1	3.52 ± 0.1	0.7 ± 0.1	
$In_xAl_{1-x}N$	0.70 ± 0.05	6.10 ± 0.1	3.4 x + 1.2	Ref. [19]

One unique lattice-matched system are $Al_{1-x}In_xN$ - GaN (x=0.174) heterostructures, which provide for a large band-offset as well as an refractive index contrast $\Delta = \left(n_{2_{GaN}} - n_{2_{AlInN}}\right)/n_{2_{GaN}}$ of 7% with respect to GaN. This lattice matched $Al_{0.83}In_{0.17}N$/GaN system is for instance explored for resonant cavity light emitting diode (RCLED) vertical cavity surface emitting laser (VCSEL)[20,21] or field effect transistor (FET)[22] devices. The bandgap energies and electron affinities of this system are however not suited for photoelectrocatalytic considerations.

8.1.2 Bandgap alignments for InN-GaN-AlN-InN alloys and heterostructures

Ternary Ill-nitride alloys are promising for photonic absorber structures in photoelectrocatalytic architectures for fuel generation from sunlight. The design and fabrication of photoelectrocatalytic structures that are based on group III-nitride heterostructures or electrolyte-semiconductor interfaces requires reliable values for the valence band positions and bandgap values of the three binaries InN, GaN, AlN, as well as the valence band- and bandgap value shifts for their ternary alloys. A wide spread of values are reported and summarized in several reviews.[8,10,11] The most recent review by Moses et al.[11] summarizes the present status on the bandgap and band alignment values and highlighted the wide range on uncertainty in the absolute values of the valence band positions, which are affected by interfacial and surface termination effects. The evolution of the bandgap values and the band alignments for the binaries InN, GaN, AlN and their ternaries are depicted in **Figure 8.2**. It shows that the energy bandgap values range from 6.1eV for AlN to approximate 0.7 eV for InN. In the ternary alloy system, the valance and conduction bands can be engineered over a wide energy range, allowing the energetic alignment of the semiconductor bands with the HOMO and LUMO levels of catalysts for efficient charge transfer. The system thus provides the possibility to investigate the photoanode behavior of low-gap compounds. For InGaN alloys with a composition of-25%-30% indium, the energy gap of 2.2eV as well as the band edge positions are such that also single junction water splitting with light could be viable.

The ternary bandgap values for the InN-GaN-AlN alloys together with bowing parameters b are given in **Table 8.2**. Pelá et al.[23] reviewed the bandgap values for the binary and ternary alloys and utilized local-density approximation LDA-1/2 method[24] to establish more accurate bandgap parameter, taking experimental data in account. The bandgap value for InN was estimated by LDA-1/2 to be 0.95 eV,[23] which is inconsistent with experimental values that converges to a bandgap value of approximate 0.70 eV. The valence-band positions relative to the vacuum level, $E_{Vac\text{-}V}$ vary strongly in literature and seem to be highly influenced by surface orientation and surface polarity.[11,10] The valence band offset between binaries InN and AlN was determined by x-ray photoelectron spectroscopy to be 1.52 eV[25] with an associated conduction band offset of 4.0±0.2 eV, forming a type-I heterojunction between the binaries. The valence-band offset between binaries InN-GaN positions was estimated to be 0.62 eV with an bandgap bowing parameter b of 1.36 eV.[19] The relative valence-band is assumed to shift linearly with composition x[19], assigning the observed bandgap bowing to a nonlinear conduction band shift.

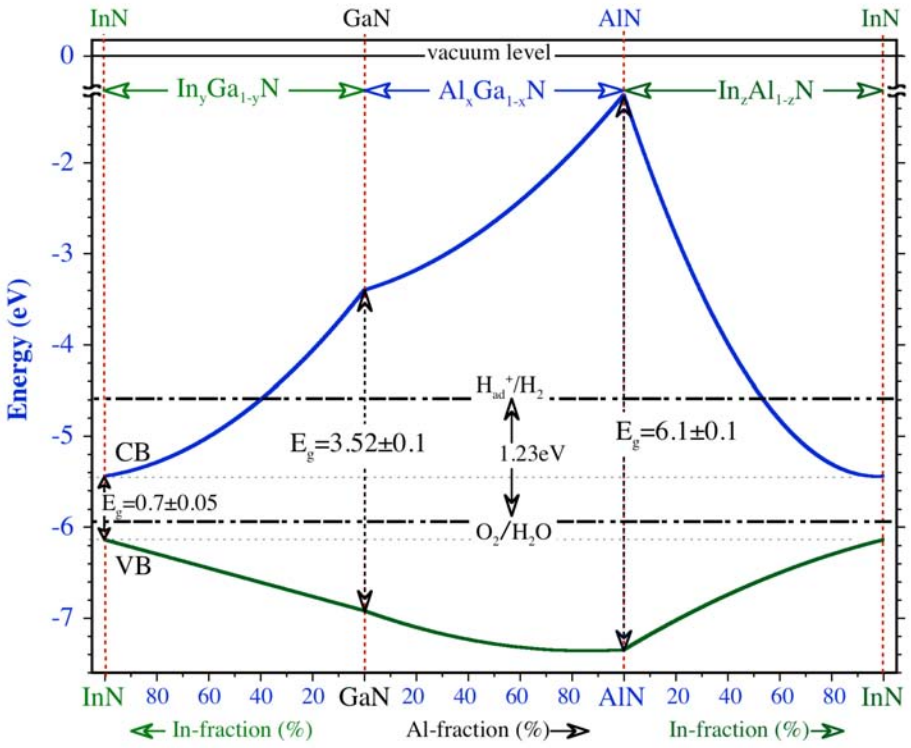

Figure 8.2

Valence band position and offsets for group III-nitrides alloys. Also marked are the hydrogen redox (H_{ad}^+/H_2 - located at about 4.6 eV) and oxygen redox ($0_2/H_20$ -about 1.23eV below) potentials for water dissociation.

Table 8.2: Valence band position and offsets for group III-nitrides alloys

Valence band position absolute to vacuum level

Alloy	$E_{vac} - E_{v\,(XN)}$	Literature
c-plane '*wz*-InN' (In-terminated)	6.03 eV	Ref. [13]
c-plane '*wz*-InN' (N-terminated)	6.41 eV	Ref. [13]
m-plane '*wz*-InN'	6.52 eV	Ref. [13]
m-plane '*wz*-InN' relaxed	5.81 eV	Ref. [11]
m-plane '*wz*-GaN' relaxed	6.42 eV	Ref. [11]
m-plane '*wz*-AlN' relaxed	6.88 eV	Ref. [11]

Valence band offsets between binaries: $E_{v\,(AN)} - E_{v\,(CN)} = E_{\Delta V\,(A_xC_{1-x}N)} \cdot x - b \cdot x \cdot (1-x)$

Ternary alloy	Valence band offset between binaries (eV)	Bowing parameter b	Literature
$In_xGa_{1-x}N$	- 0.71	0 (linear with x)	Ref. [19,11]
	- 0.85±0.15	linear with x	exp. Ref. [26]
	-0.58±0.08	N/A	exp. Ref. [27]
	- 0.78	PE on InN/GaN HJ	exp. Ref. [28]
$Al_xGa_{1-x}N$	+ 0.7xxx	0.6	Ref.
	+ 0.43	-	Ref. [11]
$In_xAl_{1-x}N$	-1.52 ± 0.17	-	exp. Ref. [25]
	-1.32	-	exp. Ref. [29]
	-0.96	-	Ref. [11]

8.2 Fabrication of epitaxial alloys and heterostructures

8.2.1 Epitaxial growth techniques

Several methods have been developed for the growth of InN, GaN, AlN, and their alloys. The choice of which method is used is based on the desired properties of the crystals. In general, two parameters must be considered: thickness and quality. The major growth methods shall be briefly discussed:

a) Low-pressure MOCVD

Metalorganic chemical vapor deposition (MOCVD or MOVPE) is a well-established growth method for the growth of AlGaN and InGaN[30]. Using nitrogen and/or hydrogen as carrier gas, metalorganic (MO) precusors are used as the metal sources (for example TMG or TEG as a gallium precursor), and ammonia (NH_3) is used as nitrogen source. Both, the metalorganic precursor and NH_3 are transported to the reaction zone above a substrate to form the desired group-III-nitride compound. Typically, MOCVD is used in the mass transport limited regime, in which the growth rate solely depends on the amount of supplied metalorganic.[31] Growth temperatures are in the range from 600°C for InN up to 1500°C for AlN (with growth temperatures for GaN lying around 1050°C). Reactor pressures may range from 100 Pa to close to 100 KPa (ambient pressure). Growth rates as high as 5 μm/hr can be achieved by MOCVD. Major impurities found are oxygen, hydrogen, carbon, and silicon.

b) Hydride Vapor Phase Epitaxy (HVPE)

This method uses the reaction between gallium trichloride ($GaCl_3$) gas, indium trichloride ($InCl_3$) gas, aluminum trichloride ($AlCl_3$) gas, and ammonia (NH_3) gas to form GaN,[32-34] InN,[35,36] AlN, and ternary III-nitride alloys. The reaction between the source gases takes place in a 2-zone temperature controlled furnace with growth temperatures in the raction zone comparable to those of MOCVD. Similar to MOCVD, the growth with HVPE takes place close to the thermal equilibrium. Due to very high gas flows that can be employed in HVPE, high growth rates of 10- 50 μm/ hours can be achieved, enabling the growth of thick bulk-like GaN and AlN layers.

c) MBE and plasma-assisted MBE

In contrast to MOCVD and HVPE molecular beam epitaxy (MBE) is kinetically driven rather than typical thermally based chemical reactions.[37,38] For the deposition via MBE the source materials (metallic gallium, aluminum or indium) are heated in a Knudsen effusion cell under ultra high vacuum. As the nitrogen source, typically a nitrogen beam from a plasma source is employed. Both, metal and nitrogen impinge and react on the substrate to form the group-III-nitride compound. MBE is a non-equilibrium growth method with very low deposition rate in the range of some hundreds of nanometers per hour. A major improvement in the growth of III-nitrides by MBE came when plasma-sources where added to growth systems to assist the activation of nitrogen precursors.

d) Remote-plasma-enhanced or reactive rf-sputtering CVD

Due to the low desorption pressure of nitrogen in InN, growth temperature for this material are comparably low (around 500°C). At these temperatures the dissociation of NH_3 to provide nitrogen for the growth of InN is reduced, leading to InN films with low nitrogen concentration. RF-sputtering CVD is using an RF plasma to enhance the dissociation of NH_3 and increase the incorporation of nitrogen.[39,40] Thus, the growth of III-nitrides can be accomplished at much lower growth temperature, while the growth rates are comparable to MOCVD. Defect levels comparable to that of MBE can be achieved.

e) Superatmospheric MOCVD (also denoted as high-pressure CVD)

This technique is an extension of MOCVD towards the superatmospheric reactor pressure regime. Promising results were achieved in the growth of InN and In-rich InGaN as this technique enables higher temperatures for these materials.[41-43] However, controlled precursor injection schemes become critical as gas phase reactions become imminent with increasing gas phase densities. An additional challenge is the reduction of the surface boundary layer with increase reactor pressure, which leads to a decreased growth rate for higher pressures. The importance of this approach lays in the reduction of the growth temperature gaps between the III-nitride binaries, which is critical for the stabilization of embedded ternary III-nitride alloys and heterostructures.

8.2.2 Substrate issues

Different substrates for the growth of group-III-nitrides are used. These include sapphire, SiC and silicon. Sapphire, the most widespread substrate, is used since it is relatively inexpensive and can be bought commercially with diameters up to 6 inches. In contrast, SiC is comparably expensive but offers more desirable properties such as better heat transport and decreased lattice mismatch[31]. Silicon use as a substrate is mainly motivated by the possibility to integrate group-III-nitrides into the well-established silicon technology, and the ease of availability of large are substrates[44]. However, especially for AlN and InN, growth on silicon is so far not well understood. All these substrates have a thermal and lattice mismatch to AlN, GaN, and InN leading to strain in the layers. Thus, native substrates, i.e. bulk AlN, GaN, and InN are widely desired. Lately, the progress in the growth of bulk GaN and AlN was tremendous, leading to the commercial availability of these substrates.[45] Unfortunately, no bulk InN crystals are available, inspiring the exploration of different concepts such as strain relaxing interlayers.[46] In the future, a strongly improved quality is expected from layers and devices grown on these bulk crystals, especially for In-rich InGaN and Al-rich AlGaN.[47-50]

8.3 The $Al_xGa_{1-x}N$ system: from the binaries to ternary alloys and heterostructures

The $Al_xGa_{1-x}N$ system represents the wider bandgap part of the III-nitride family. Certainly, GaN has been the most researched member of this family, allowing for successful device applications and future directions. Recently, interest in UV optoelectronics and high power electronics has led to focused research in the $Al_xGa_{1-x}N$ alloys, as it provides for a suitable material system for the realization of these applications. As the bandgap range of this system covers the UV part of the spectrum, they are not particularly useful for the development of photovoltaic (PV) cells or photoelectrocatalytic solar fuels. Nevertheless, they present a proper test system for the development of the general concepts for nitrides and in general the universality of point defect control in such wide bandgap materials. The following section will summarize the basic properties of the GaN and AlN binaries focusing on their polarity applications, and surface morphology. In addition, it will discuss the important thermodynamic implications for describing the full miscibility of the $Al_xGa_{1-x}N$ alloy system and its demonstration in term of MOCVD growth of these alloys. Finally, it will finish with a discussion of the current understanding of point defect with the ultimate goal o controlling their electronic properties. This is currently one of the most researched areas within this material system.

8.3.1 Properties of epitaxial GaN – AlN alloys

AlN and GaN possess a number of interesting physical, optical, and electronic properties that allow the fabrication of novel devices. III-nitrides typically form a hexagonal wurtzite unit cell and are partially ionic solids due to large differences in the electronegative of the III-metal cations and nitrogen anions. Due to the largely ionic behavior of the III-N bonds, the unit cell of the III-nitrides is distorted from the ideal wurtzite unit cell, and a large spontaneous polarization exists along the *c*-axis. As the III-metal cations have different ionic radii and bonding energies with nitrogen, the III-nitrides have different lattice constants, spontaneous polarizations, bandgap energies, and electron affinities. The non-centrosymmetric crystalline structure and the lack of inversion symmetry along the *c*-axis gives rise to two distinct polarities of the {0001}-surfaces. The cation and anion atoms are arranged in separate layers along the basal planes to form hexagonal close packed planes, and the orientation of the bonds between the cation and anion layers defines the polar orientations: III-polar (+*c* orientation) if the single bond points from III-metal cation to nitrogen anion along the <0001> direction or N-polarity (-*c* orientation) if the single bond points from nitrogen anion to III-metal cation (**Figure 8.3**). Polar orientation should not be confused with surface termination, as each orientation may be terminated with either species. The direction of the spontaneous polarization vector and the type of charge induced at a surface or interface is also determined by the polar orientation (**Figure 8.3**). As the spontaneous polarization constitutes a non-zero dipole moment per unit volume in the crystal, there exists an internal electric field in the order of a few MV/cm.[51] These internal electrical fields can enhance electron or hole accumulation at surfaces or interfaces and surface charge densities on the order of 10^{13} cm^{-2} can be generated. In addition to a spontaneous polarization, large piezoelectric polarization is present in strained crystals such as thin films deposited by heteroepitaxy. The combined effects of spontaneous and piezoelectric polarization in III-nitrides can strongly influence the electrical behavior of a device and makes the control of polarity a necessity for device fabrication.

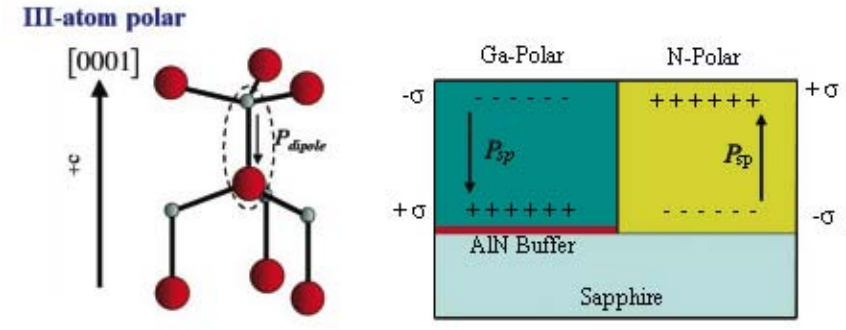

Figure 8.3: The vector direction of spontaneous polarization, Psp, in III-nitride crystals relative to the <0001> direction. The signs of the interface/surface charge, σ, are also indicated for Ga-polar and N-polar GaN grown using a patterned AlN buffer to control film polarity.

As most III-nitride growth is preformed on {0001} surfaces, the two polarities present different challenges to crystal growth due to differences in surface configurations, compositions, and chemistries[2]. These dissimilarities lead to different incorporation of impurities and the formation of difference microstructures. The principle technique for polarity control during heteroepitaxial deposition is to produce a substrate surface that favor the nucleation of grains with the preferred polarity through the use of polar substrates (Si-polar or C-polar SiC) or combinations of surface treatments for non-polar substrates (sapphire).[52,53] For GaN deposition on c-sapphire wafers, a surface nitridation with ammonia at high temperature yields N-polar GaN while the deposition of a low-temperature AlN buffer layer yields Ga-polar GaN.[53] Using

conventional lithography techniques to pattern and selectively etch a low-temperature AlN buffer layer of ~30 nm thickness deposited on a sapphire wafer allows for Ga-polar and N-polar domains to be grown simultaneously (see **Figure 8.4:**).[53] In the case of homoepitaxial deposition, the polarity of the deposited film is inherited from the substrate.

In addition to requiring polarity control techniques, epitaxial deposition of the III-nitrides presents other challenges. The large lattice mismatch between the different III-nitride materials and other common substrate materials result in dislocation densities of 10^9-10^{10} cm^{-2} for heteroepitaxially deposited thin films. With such large dislocation densities, many of the electrical and mechanical properties are impacted. The surface morphology of heteroepitaxy III-nitride films is also controlled by dislocations, and III-nitride crystals grown in supersaturated environments develop bi-layer step spirals emanating from screw dislocations.[54] **Figure 8.4**a shows an atomic force microscopy (AFM) image of a GaN thin film deposited by metalorganic chemical vapor deposition (MOCVD) on *c*-sapphire. The spacing between successive bi-layer steps in a growth spiral can be controlled through process supersaturation during deposition and can be varied from ~100 nm to ~200 nm.[55] In contrast, homoepitaxial and pseudomorphic heteroepitaxial films inherit a much lower dislocation density from their substrate material, typically 10^6 cm^{-2} for GaN and 10^4 cm^{-2} for AlN substrates.[56,57] The surface morphology of films with reduced dislocation densities is more alike to single crystalline surfaces and is determined by surface energy minimization.

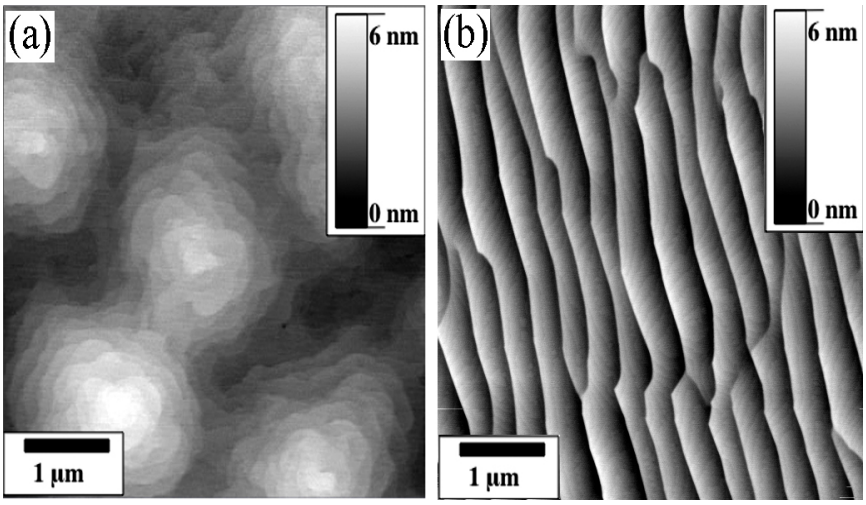

Figure 8.4:
a) 5×5 µm^2 AFM images of (a) Ga-polar GaN film deposited on *c*-sapphire and (b) Al-polar AlN deposited on bulk AlN with a miscut of about 1 deg. The bi-layer step spacing is approximately 150 nm for both samples. The GaN bi-layer steps are arranged in spirals emanating from screw dislocations. The AlN surface show step-bunches of 3 nm height with a spacing of 350 nm.

Figure 8.4b shows an AFM image of an AlN thin film deposited by MOCVD on bulk (0001)-AlN with a miscut of about 1° where a combination of crystalline faceting and bi-layer steps are evident. This morphology is the result of step-flow growth by individual bi-layers and step-bunching of these bi-layers to form alternating (0001)-AlN facets and high Miller-index or unreconstructed facets to conserve the macroscopic misorientation of the AlN substrate[58]. As with heteroepitaxial films, the spacing of the bi-layer steps of homoepitaxially deposited AlN can be controlled by process supersaturation during deposition and can be varied from 90 nm to 150 nm.[59] The spacing of the step-bunches can be varied from 80 nm to 500 nm by varying the miscut of the AlN substrates. The capability of using AlN single crystalline wafers for homoepitaxial growth of AlN and pseudomorphic Al-rich AlGaN films was recently developed. This capability arises from the development of the technology for growth and wafering of bulk single crystal AlN grown by physical vapor transport.

The III-nitrides show promise for use in photochemical processes due to the large range of electron affinities. It is generally accepted that the electron affinity of GaN is 4.1 eV. Reported values of the electron affinity of AlN and InN are ~2 eV and 5.8 eV but are topic of on going research.[60,61] As discussed in section 8.1, the electron affinities of ternary alloys have a high uncertainty, but they are expected to exhibit electron affinities intermediate to the binaries.

8.3.2 Ternary AlGaN alloys and heterostructures

The enthalpy of mixing for III/V (including III-N), IV, and II/VI semiconductor solid solutions is always positive at temperatures below a certain critical temperature.[62] A positive enthalpy of mixing in terms of atomic interactions indicates a "higher bond energy" between two distinct species due to "chemical" energies (related to partial charge transfer due to differences in electronegativity), and "strain" energies related to distortions in the lattice due to differences in the sizes of the constituent species. This could bring about that a single, homogeneous solid phase has a higher free energy than a mixture with two solid phases.

The regular solution model satisfies the condition of a non-zero enthalpy of mixing. A regular solution, as defined by Hildebrand, is a solution with a non-zero enthalpy of mixing and no excess entropy of mixing, suggesting neither clustering or ordering.[63] This model is used to predict the stability of the different AlGaN solutions within a pseudobinary phase diagram. Following the regular solution model, the molar free energy of mixing for $Al_xGa_{1-x}N$ is given by:

$$\Delta G_M = \Omega x(1-x) + RT\left[x\ln x + (1-x)\ln(1-x)\right] \quad (1)$$

where R is the molar gas constant, x is the AlN molar fraction within AlGaN, and Ω is the interaction parameter. Using a modified valence-force-field model (VFF), Ho et al. calculated the interaction parameter to be 3.6 kJ/mol with the main contribution coming from the microscopic strain energy associated with the bond distortion in the alloy.[64] Figure 8.5 shows the molar free energy of mixing dependence on the molar fraction of AlN within the solid solution of $Al_xGa_{1-x}N$ for three different temperatures characteristic of the processing of these alloys. For these temperatures, all composition ranges within the free energy curve have lower free energy of mixing than the extremes of the ranges. There are no binodal points that would define a binode (where a homogeneous phase will be metastable or unstable). The binodal critical points are defined by the extreme or critical points of the molar free energy of mixing, that is, $d\Delta G_M/dx = 0$, defining the binodal curve. The critical temperature, the temperature at which at any temperature above the solid solution is stable, is -56°C, well below the processing temperatures of these alloys. A binode region exists within the pseudobinary phase diagram of the AlGaN alloy below this temperature. All alloy compositions will be stable against phase separation and segregation above this temperature (for temperatures used during processing).

The stability of these alloys is demonstrated by growing layers of different Al composition by metalorganic vapor phase epitaxy (MOVPE). As mentioned above, all alloy compositions are expected to be stable against phase segregation under common growth conditions. The concentration of Al in the alloy is simply given by $x_{Al} = f'_{Al}/f'_{Ga} + f'_{Al}$ where f'_{Al} and f'_{Ga} are the actual fluxes arriving to the growing surface of the corresponding Al and Ga carrying species. These actual flows can be related to the intended flows as $f'_{Ga} = \alpha f_{TEG}$ and $f'_{Al} = 2\beta f_{TMA}$ where f_{TEG} and f_{TMA} are the corresponding triethylgallium (TEG) and trimethylaluminum (TMA) intended metalorganic flows. In this definition, the factors α and β are introduced as correction

factors and the factor of 2 in the Al flow is due to TMA being a dimer in the gas phase at room temperature. From this, concentration of the Al alloy can be written as:

$$x_{Al} = \frac{2\beta f_{TMA}}{\alpha f_{TEG} + 2\beta f_{TMA}} = \frac{2\frac{\beta}{\alpha} f_{TMA}}{f_{TEG} + 2\frac{\beta}{\alpha} f_{TMA}} \tag{2}$$

where a correction factor ratio can be defined as $\gamma = \beta/\alpha$. After this definition, the aluminum concentration in the alloy should be expressed as:

$$x_{Al} = \frac{2\gamma f_{TMA}}{f_{TEG} + 2\gamma f_{TMA}} \tag{3}$$

taking the correction factors into account.

Pre-reactions or parasitic reactions in the gas phase are expected for aluminum and ammonia within the MOVPE process, since it is a spontaneous and strongly exothermic reaction. This depletes the source flow of the aluminum component, artificially increasing the gallium fraction within the alloy.[65] In order for equation (3) to be satisfied if the pre-reaction occurs, the reduction in the aluminum flow or the reaction rate needs to be linearly proportional to the aluminum concentration in the source gas flow. This implies that the pre-reaction needs to be of the first order with respect to aluminum within its kinetic rate law. Any deviation from the trend described by equation (3) will represent either an instability in the AlGaN alloy or a different order kinetic rate law. The two effects cannot be distinguished from just a deviation from equation (3).

The γ correction factor depends on particularities of the process, specifically on: temperature, total pressure, ammonia partial pressure and gas velocity through the total flow. These parameters influence the pre-reaction rate that depletes the aluminum flow.[66] In addition, these parameters determine the gallium and aluminum supersaturation, which ultimately determines the incorporation rate. Certain conditions, like high temperatures (above 1100°C) and low ammonia partial pressures may lead to low gallium supersaturation, inducing a deviation from linearity.

Figure 8.6: shows the AlN molar fraction within the AlGaN alloy as a function of the ratio of the molar flow rates as given by equation (3). Only one composition was observed per intended film. The Al compositions graphically represented this way can be fitted with a line of slope 1, if the γ factor is equal to 1.4, throughout the whole composition range, from 0 to 1. As mentioned above, this implies that the alloy compositions are stable against phase separation and segregation. In addition a γ factor greater than 1 implies that no significant amounts of aluminum (if any) are being lost to pre-reactions. This is dependent on the particular process conditions and reactor geometry used to grow the films.

The film relaxation is defined as $R = (a - a_S)/(a_R - a_S)$, where '$a$' is the measured in-plane film lattice constant, 'a_R' is the relaxed in-plane film lattice constant, and 'a_S' is the in-plane substrate lattice constant, that in this case is a for GaN, is easily determined. A relaxation of 0 indicates a fully coherent interface between film and substrate, while 100% relaxation implies a fully relaxed film.

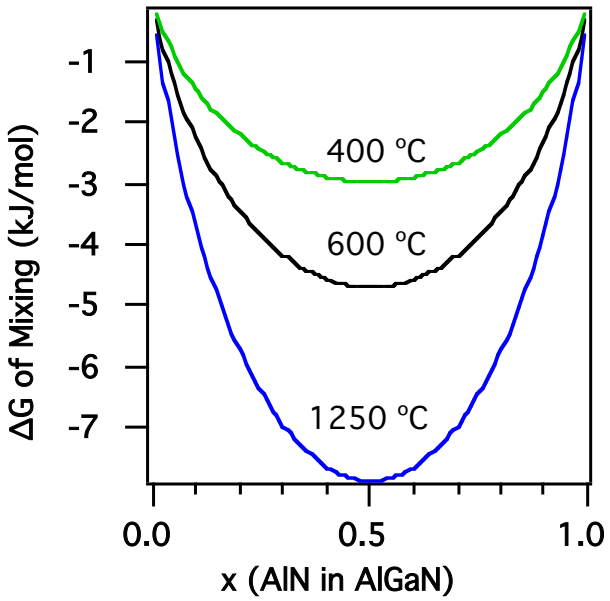

Figure 8.5: Molar free energy of mixing for AlGaN as a function of the molar fraction of AlN within AlGaN for three different temperatures.

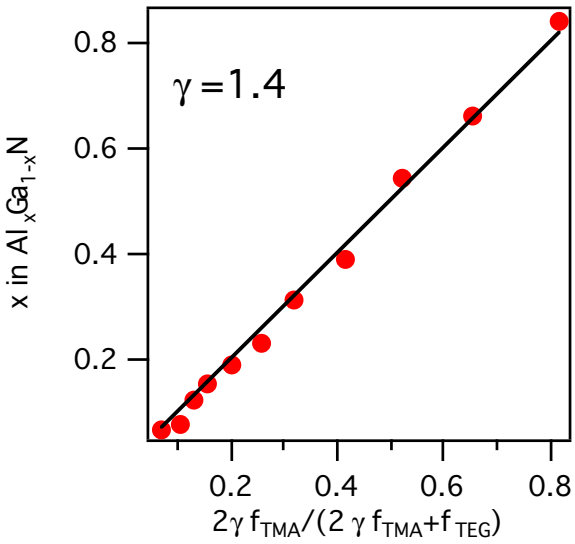

Figure 8.6: AlN molar fraction within the AlGaN alloy as a function of the ratio of the molar flow rates as given by equation (3).

Figure 8.7 shows the film relaxation as a function of the AlN molar fraction within the AlGaN alloy. For compositions below 20%, the relaxation is 0, implying a fully coherent interface, while for composition around 20% there is a slight degree of relaxation, reaching 12%. Nevertheless, there is an abrupt transition at about 25 to 30% in Al content, where the film achieves nearly full relaxation (for composition above 30% to below 60%) and full relaxation for compositions above 60%. This abrupt change in the relaxation as a function of composition is indicative of cracking as the relaxation mechanism. AlGaN films on GaN are in tension since the in-plane lattice constant of AlGaN is smaller than that of GaN. Extensive cracking is observed on the higher Al-content AlGaN films.

Figure 8.8 shows a 2θ–ω triple crystal scan on the direction normal to the substrate for the films represented above. The reflections from the (0002) planes from GaN and AlGaN can be observed along with Pendellösung thickness fringes around the AlGaN peak for AlGaN films with compositions below 25% Al. The occurrence of these fringes has been qualitatively related to the high quality of these films.

Although the previous discussion relates to AlGaN films on GaN templates, recent work describes the progress of AlGaN on AlN bulk crystals substrates. Dalmau et al describes this state of the art for this system, AlGaN films with compositions above 60% Al remain pseudomorphic for thickness below 1 μm.[47] Partial relaxation is observed, but not via the cracking mechanism as these films are expected to be in compression, contrary to those grown on GaN that are expected to be in tension.

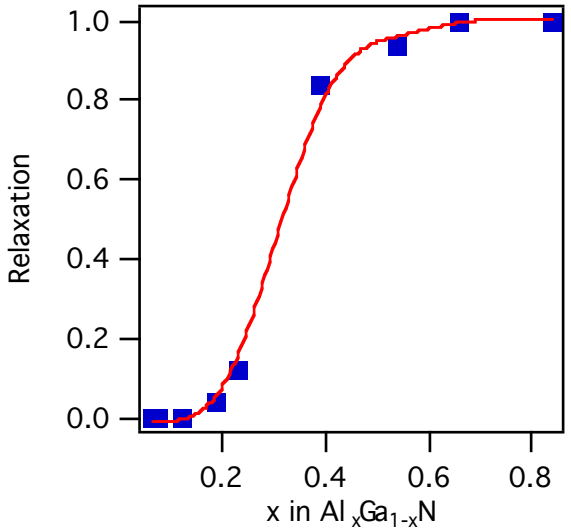

Figure 8.7: Film relaxation as a function of the AlN molar fraction within the AlGaN alloy for a film thickness of 200 nm.

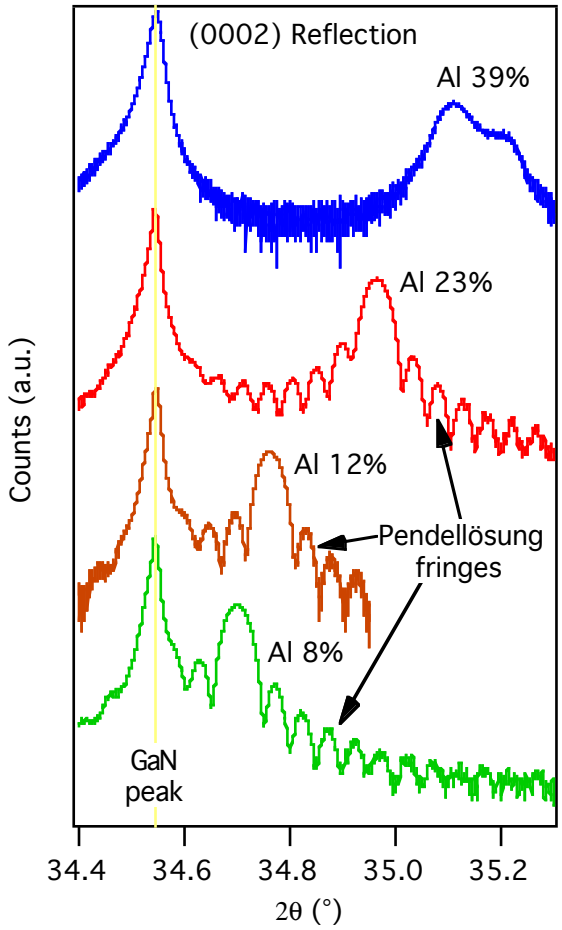

Figure 8.8: 2θ-ω triple crystal scan of the AlGaN/GaN films grown on sapphire.

8.3.3 Point Defects in AlGaN alloys: Electrical Properties

Three types of point defects have been identified as determining the conductivity properties of n-type AlGaN: Si, O, and V_{III}. Silicon is commonly used as the impurity of choice for intentional doping of n-type AlGaN. It is readily incorporated as a substitutional impurity with a charge state (q) of +1 in a III-site, acting as a donor, covering the whole alloy range, from GaN to AlN. The intrinsic energy of formation of this impurity has been estimated as - 0.8 eV and less than –1.5 eV for GaN and AlN, respectively.[67] Activation energy of 17 meV at a donor concentration of $3x10^{17}$ cm^{-3} has been observed in GaN. For AlN, higher values than that predicted by a hydrogenic model (75 meV) have been reported, but these measurements do not take into account the high degree of compensation observed. The activation energy of Si for $Al_{0.7}Ga_{0.3}N$, after taking into account the high degree of compensation, was measured to be 55 meV with a predicted (hydrogenic model) value of 60 meV.[68] Thus, it is reasonable to assume that the actual value for the activation energy of Si in AlN is around the predicted value (from 75 meV to 95 meV). These activation energies correspond to activation ratios of 0.5 to 0.06 in GaN and AlN respectively. For the alloy compositions of technological interest, the activation ratio is expected

to be around 0.1. At high Si incorporation it has been discussed that Si may occupy a N-site, self-compensating the free carriers. The intrinsic energy of formation of Si in a N-site (Si_N) is much higher than that of the Si_{III} due to the size mismatch with N, making its formation highly unlikely and thus it cannot be considered as an amphoteric dopant[69]. Highly conductive n-type $Al_{0.7}Ga_{0.3}N$ has been achieved by heavy doping with Si ($6x10^{19}$ cm^{-3}) yielding a carrier concentration of ~$1x10^{19}$ cm^{-3} and mobilities of ~25 cm^2/Vs.[2] Lower activation energies are observed by bandgap renormalization due to the heavy doping.

For the next point defect, oxygen is a common impurity in III-nitrides that is unintentionally incorporated during growth. Similar to Si, it is readily incorporated as a substitutional impurity with a charge state (q) of +1 in a N-site, acting as a donor. The intrinsic energy of formation of this impurity has been estimated as 0.3 eV and –0.1 eV for GaN and AlN, respectively. This impurity has been attributed to be the cause of the n-type background carrier concentration observed in GaN. On the other hand, O is expected to undergo a *DX* transition at $x > 0.3$ in $Al_xGa_{1-x}N$ that can act as a deep acceptor, effectively compensating intentional donors in the semiconductor.[70,71] Experimental observations suggest that this transition may not occur up to x ~ 0.6 from observations of unintentionally doped n-type $Al_{0.67}Ga_{0.23}N$ with resistivity of 85 Ω cm at room temperature[72]. This indicates that the intrinsic energy of formation of this defect is slightly higher than expected, thus complete compensation from O in the alloy range of interest is not expected, although some compensation is still present.

III-Vacancies is the last important point defect that needs to be taken into account. Three charged states (-1, -2, -3) and one neutral state could be stable in the system, along with their corresponding complexes with oxygen.[73-75] In both cases, the three charged states act as ionized acceptors, strongly compensating intentional donors. As discussed above, native compensation as provided by these vacancies and their complexes are the main source of compensation for n-type wide bandgap semiconductors. The formation energy of these defects gets lowered as the bandgap increases. It is important to note that the intrinsic energy of formation of vacancies or their complexes is lowered near a dislocation due to the presence of the associated strain field, in other words the equilibrium concentration of these defects increases near a dislocation. Therefore, reduction of dislocations is desirable to further enhance the electrical conductivity in n-type material.

Magnesium is the p-type dopant of choice for AlGaN alloys. It is readily incorporated in a III-site as an acceptor, while it is energetically unfavorable to be incorporated on an interstitial site or a N-site. A high ionization energy (around 150 meV for GaN as presented in previous reports) yields low hole concentrations. In AlN, this energy is expected to be around 400 meV, thus for the AlGaN compositions of technological interest yields an activation ratio of $1x10^{-5}$.[76] In this case, high incorporation of Mg are needed to achieve technical conductivities in p-type AlGaN.

Similar to the scenario presented above for n-type AlGaN, native compensation with N vacancies as a donor of different ionization states is a fundamental problem in p-type doping. In the case of a N vacancy, the intrinsic energy of formation is around 1.5 eV to 2 eV for GaN and AlN, respectively. These energies are lower than that for a group-III vacancy, making their formation highly favorable. Taking into account the lowering of the energy of formation as the Fermi level moves to the top of the conduction band, should make the existence of p-type material impossible. It has been established that the mechanism responsible for p-type conduction in a standard process is the possibility of co-doping with hydrogen. As hydrogen is present in a typical growth environment, it readily forms a complex with Mg, which is incorporated as a neutral specie. This in turn does not alter the position of the Fermi level, not

lowering the energy of formation of the compensating native point defect, practically inhibiting its formation. Further post-processing of the layer is used to remove the hydrogen and activate the Mg as a p-type dopant. This processing is performed at temperatures high enough for possible complex dissolution and diffusion but low enough to kinetically inhibit the otherwise favorable formation of the N vacancies. In other words, we can think of p-type material as a kinetically stabilized property.

Other species have been theoretically and experimentally explored as alternatives to Mg doping, but still Mg remained as the best alternative. Other IIA and B family species suffer from low solubility due to higher size mismatch and higher ionization energies. Be has been explored as a realistic alternative, with similar ionization energies as Mg and higher solubility due to its reduced size. But that reduced size facilitates incorporation as interstitial specie where it acts as a donor, thus causing self-compensation [77]. Since no better alternative to Mg seems possible, current research focuses on establishing process routes to inhibit the formation of the native compensating defects without using H as a co-dopant, maximizing in this way the p-type carrier concentration possible from the incorporated acceptor.

8.4 The $In_xGa_{1-x}N$ system

Even though group III-nitride alloys have been investigated for several decades, the breakthrough for the material system came with improvements in the GaN thin film growth technology and the successful demonstration of the first InGaN based blue LED [78] and laser diode [79], which delivered on the promise of a blue solid state light source with the potential of an all spectral tunable LED based on InGaN alloys. The vision became even more prominent with revelation of the low bandgap value of InN (Eg = 0.7eV), which made the InGaN alloys system also of interest for optical communication application and multi-junction photovoltaic (PV) solar cells. The following section will provide a short review on the present state of materials growth and materials structures formation, leading towards emerging materials- and device structures.

8.4.1 Gallium-rich ternary InGaN alloys and heterostructures

The binary GaN discussed in sect. 8.3, is one of the most studied group III-nitride binary. Tuning the optical bandgap between the binaries GaN and InN from the UV to the mid IR wavelength region depends on the ability of incorporation of indium into the InGaN lattice, maintaining a common processing window during the growth process.

Therefore, one of the most important topic during the recent years was to understand the influence of nanoscale and microscopic fluctuations in the indium content on the structural, electrical and optoelectronic properties of ternary epilayers and MQW structures.

The incorporation of indium into the InGaN alloys and the growth of InGaN/GaN MQW's are affected by several factors:

a) The presence of spontaneous and piezoelectric polarization-related electric fields that occur parallel to the c-axis of wurtzite InGaN growth surface. Heterostructures grown along the c-axis may therefore exhibit large internal electric fields that affect the radiative recombination rates as well as the carrier transport of the heterostructure barriers. [80]
b) The polar nature of wurtzite III-nitride materials leads to two growth surface polarities which challenges growth process due to differences in growth surface chemistries, impurity incorporation and surface morphology evolution. The control of the surface polarity is therefore essential for the structural, and physical layer properties.

c) The large lattice mismatch between the different III-nitride materials and other common substrate materials result in dislocation densities of 10^9-10^{10} cm^{-2} for heteroepitaxial layers. Such large dislocation densities impact the structural, mechanical and optoelectronic layer properties.
d) The vastly different partial pressures between the binaries leads to significant different growth temperatures for InN, GaN, and AlN, challenging the stabilization of their ternaries and quaternaries at optimum processing conditions.[81] Lateral spinodal decomposition within the growth surface is expect to contribute to the phase separation due to the miscibility gap in InGaN alloys grown under low-pressure MOCVD and MBE growth conditions [82].

To address issues related to piezoelectric field at interfaces, the recent review by Farrell et al. [80] summarized growth efforts on nonpolar and semipolar GaN templates and the effect of the substrate misorientation on growth surface morphology and device performance. Recent advances in understanding and controlling the extending defects in such structures led to improved high-performance LDs on freestanding $(20\bar{2}1)$ GaN substrates. However issues related to compositional induced lattice-strain as well as the stabilization of the different partial pressures between the binaries InN and GaN have to be solved to utilize the full compositional range.

8.4.2 InN and indium-rich InGaN epilayers and heterostructures

The growth on InN and the integration of higher indium concentrations of InGaN into ternary III-nitrides is a major challenge with the presently employed low-pressure deposition techniques such as MBE and low-pressure metal-organic chemical vapor deposition (LP-MOCVD) due to thermodynamic limitations of stabilizing materials with vastly different partial pressures.[81,83] For instance, in order to integrate InN or indium-rich InGaN epilayers into GaN or gallium-rich InGaN heterostructures, a common growth processing window has to be establish under which different compositions of InGaN can be stabilized. However, the presently established LP-MOCVD processing conditions revealed a temperature gap of almost 400°C between InN and GaN, which has to be bridged by any kind of off-equilibrium means of growth surface stabilization. If the growth process itself does not provide sufficient growth surface stabilization, the growth temperature difference between the two binaries provides a significant driving force of the structural degradation of the layer quality and the predicted miscibility gap in the ternary InGaN alloys.[84,82] Consequences associated with this problem are discussed in the context of spinodal decomposition, compositional fluctuations and phase segregations in the ternary InGaN[85-92,10] system - an added problem to compositional induced lattice strain, interfacial piezoelectric polarization effects, and extended defect related effects that have to be addressed.

To address the stabilization of InN and indium-rich III-nitrides, off-equilibrium growth techniques such as plasma-assisted MBE[37,38] or remote-plasma-enhanced CVD[39,40] concepts are explored. A further expansion of the processing space is assessed by superatmospheric or high-pressure CVD[41-43]. High-pressure or superatmospheric MOCVD extends the growth parameters space by enabling reactor pressures of up to 100 bar.[42,93,94] Growing indium-rich InGaN at elevated pressures allows an increase of the growth temperature of an compound with highly-volatile constituents, closing the growth temperature gap between the binaries. Therefore, utilizing the reactor pressure to stabilize the growth surface is a viable approach to overcome problems of off-equilibrium techniques arising from different partial pressures and low growth

temperatures. Recent research on HPCVD growth of InGaN has demonstrated the this approach reduces the gap in the growth temperature processing window of group III-nitride alloys.

As depicted in **Figure 8.9**, the growth temperatures of InN can be increased by more than 120°C in the pressure regime between 1 and 20 bar, which is a significant advantage over conventional low-pressure MOCVD, where the growth temperatures are around 650°C. For InGaN, the increase of growth temperature as function of reactor pressure decreases due to the reduced temperature gap between InN and GaN. Therefore the MOCVD reactor pressure (high-pressure versus low-pressure) is critical balance between the partial pressures of the alloy compositions that have to be integrated / stabilized at a specific growth temperature.

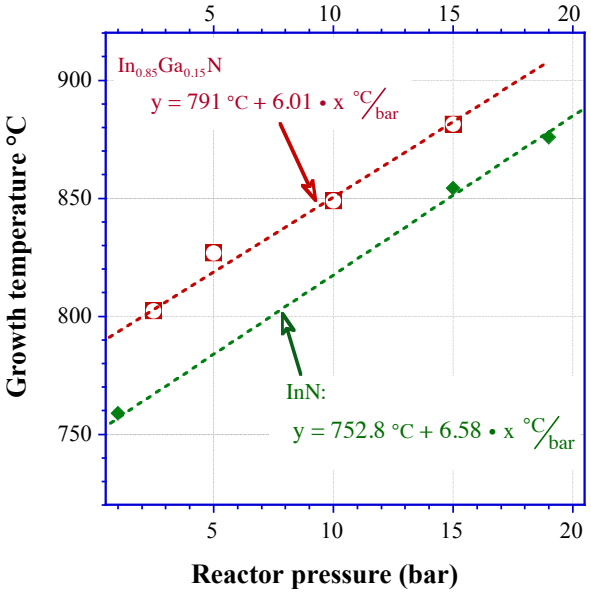

Figure 8.9: Growth temperature versus reactor pressure for the growth of InGaN epilayers under HPCVD growth conditions.

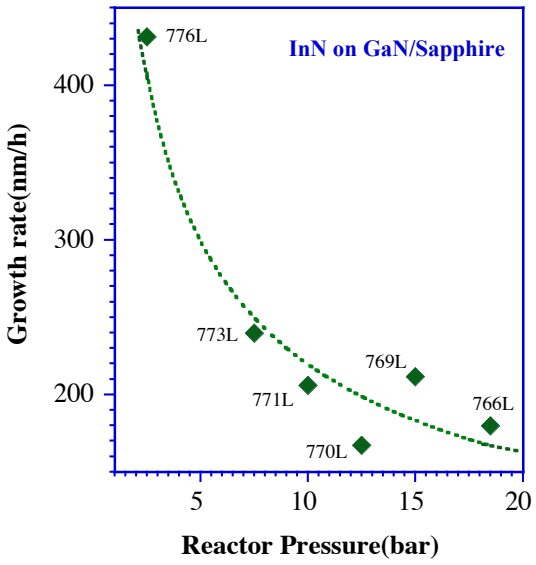

Figure 8.10: Decrease of growth rate with increasing reactor pressure for InN growth.

A major drawback of the high-pressure CVD approach lays in the significant reduction in growth rates with increasing reactor pressure as depicted in **Figure 8.10**. In the investigated pressure range of 20 bars, the growth rate falls almost by one order of magnitude, suggesting that even if this approach is feasible to stabilize and integrate MQW with vastly different partial pressures, it might not viable for thick material layer growth. As demonstrated, the stabilization of indium-rich InGaN can be addressed by the high-pressure CVD,[95,96,94,97,42] using a pulsed injection of the precursor scheme, which minimizes gas phase reactions and has the significant advantage to prevent phase segregations. This scheme facilitates the control of the growth process on a sub-monolayer level and enables a thorough real-time optical analysis of surface chemistry processes during growth. Present research explores the phase stability of InGaN and the digital InGaN alloy formation, which may not only prevent phase segregations but also enables the fabrication of III-nitride superlattices.[98-100]

Grandal et al.[100] showed that multiple quantum wells (MQWs) of $In_{0.83}Ga_{0.17}N$-InN-$In_{0.83}Ga_{0.17}N$ grown on GaN can be fabricated by plasma-assisted molecular beam epitaxy (PA-MBE) with light emission at 1.5 micrometer. The PA-MBE approach uses the kinetic energy of the incoming atoms/ions to stabilize the growth surface, using relative low growth temperatures

(below 500°C). Both PA-MBE and HPCVD have the same goal of controlling the partial pressure at the surface to integrate dissimilar materials - but different process control parameters. A critical issue is the type of growth mode: 2-dimensional (2-D) versus 3-dimensional (3-D) film growth. In 2-D growth mode, material is deposited layer-by-layer. Conversely, 3-D growth consists of formation of islands and their subsequent coalescence. The latter results in grain boundaries that detrimentally influence the topographical and electrical properties of the deposited epilayers , e.g., carrier mobility and free carrier concentration.[101]

The control of topographic properties of InGaN layers (i.e., a smooth surface) are essential for the fabrication of heterostructures and the integration of multiple quantum wells MQWs and engineered assembled nanocomposites. The unique temporal precursor injecting system utilized in the high-pressure CVD approach is promising for controlling the growth surface chemistry processes to stabilize indium-rich InGaN alloys difficult to achieve otherwise. However, the alloys may exhibit new defects related to ordering processes in a microscopic scale, which requires careful analysis as they affect the overall quality of the gain media. One of the present challenges in the epitaxial growth of ternary III-nitrides is the potential segregation of one of the constituent column III element (Ga or In) at the growth front and at the interfaces with the binary material. The ejection of indium from an underlying InGaN layer with Ga deposition thus results in a lower free energy for the surface. The transport of indium to the surface is mediated by the surface exchange of Ga for In. The lower free energy of the GaN layer accounts for the asymmetry in the In diffusion profile with growth order in compositional modulated structures. This preferential segregation has to be carefully controlled and suppressed for the growth of InGaN/InN/InGaN quantum wells (QW) and multiple quantum wells (MQWs). A further aspect arises from the strong polarity of Group III-nitride crystals. A higher concentration of indium in InGaN/InN/InGaN QW/MQWs results in more strain and more polarization.[102] The quantum confined Stark effect (QCSE) is caused by spontaneous polarization and by a strain induced piezoelectric field. Increasing the indium composition increases the piezoelectric field.[103] The resulting QCSE will cause a blue shift at high current densities moving further away from the desired wavelength, and at lower current densities efficiency will be low due to charge separation.[103-105]

Recent results showed that high-pressure MOCVD is viable to address the challenges in the growth and stabilization of indium-rich InGaN alloys – even though much more work needs to be done to improve the structural and physical properties of these alloys. At this point, the assessed thermal stability window of indium-rich InGaN alloys focused at growth temperatures in the range of 850 - 950°C, reactor pressures from 1 to 18 bar, and simultaneous group-III precursor injection. The XRD analysis for selected indium-rich InGaN summarized in **Figure 8.11** shows that a macroscopic single-phase material can be obtained. The broadening of the InGaN(0002) Bragg reflexes (see **Figure 8.11:**) and the rocking curve with FWHM's around 3000 arcsec for x=0.31 indicates a high density of point- and extended defects in these layers. The structural degrading with increasing gallium incorporation is presently addressed by exploring a sequential group-III precursor injection approach, adjusting the surface chemistry to each group III element (Ga and In) separately.

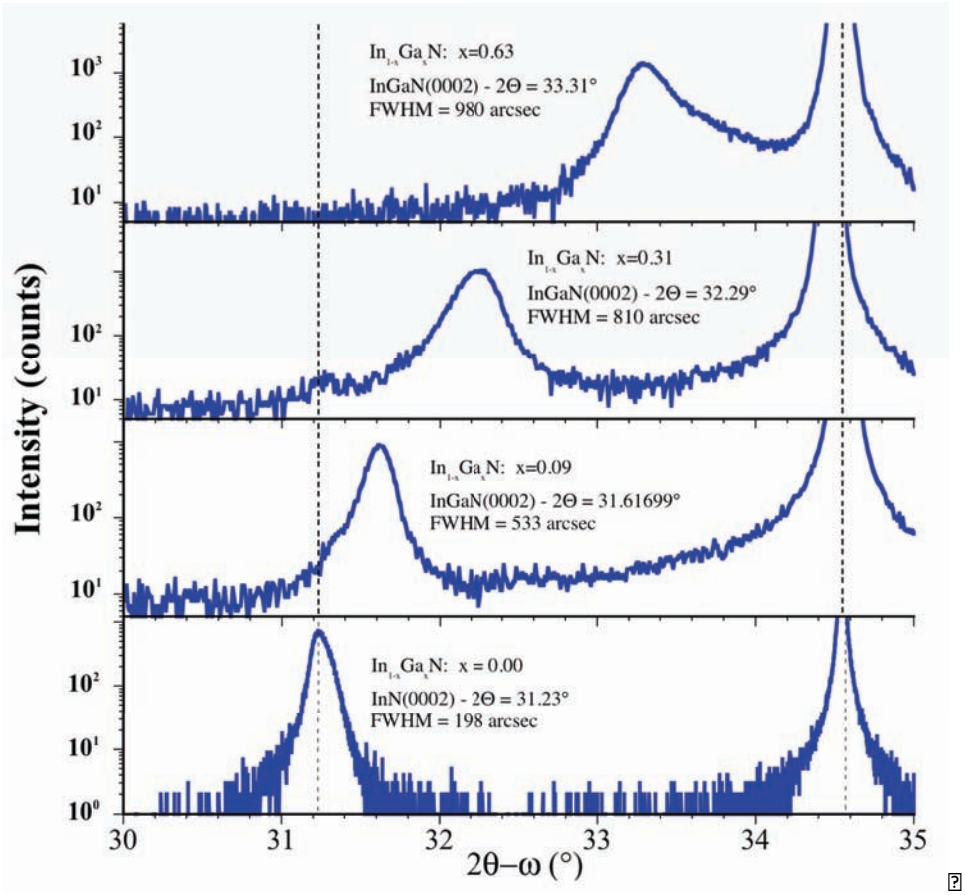

Figure 8.11:

Structural quality of InN and indium-rich InGaN alloys grown by HPCVD.

8.5 Present challenges in materials improvement and materials integration

The development of native substrates, either GaN or AlN, have led to the realization of high crystalline quality AlGaN for the eventual characterization and classification of the main factors that determine the alloy properties. For AlGaN films with Al content below 50%, a GaN native substrate is preferred, while for high Al content, AlN is the substrate of choice. Besides these recent developments, work based on heteroepitaxy on foreign substrates (i.e. Si and SiC) is still ongoing due to other factors, such as availability and other market pressures. Nevertheless, research in these native substrates actually frames the work of the other foreign substrates, as the observed reduction in dislocations bring about what otherwise may be more important limitations in the technology; without the films high crystalline quality these limitations cannot be properly distinguished and identified.

As discussed in section 8.3, due to the magnitude of their bandgap, the direct applicability of AlGaN to photovoltaic (PV) cells or photoelectrocatalytic solar fuels is limited. On the other hand, integration within the InGaN or AlInN system as part of more complex device structures, such as cladding layers or current injection layers, make them useful materials as a whole for the complete III-nitride family. In light of this, integration with the complete systems becomes rather difficult as typically the three ternary alloy systems are grown on completely different process regimes. Even thought the AlGaN alloy system is stable over the whole composition range, the InGaN and specially the AlInN system have miscibility gaps within their phase diagrams limiting the process possibilities and integration capabilities. Several new process alternatives are

being explored, some of which where discussed in the previous sections. These alternatives, especially those exploiting kinetical limitations, will open the process space for realizing these novel structures based on the nitride material system.

The main problem the AlGaN technology is currently facing is the possibility of efficient doping for n- and p-type behavior. This is a fundamental problem with wide bandgap materials that arise from two related aspects to the magnitude of the bandgap: dopant activation energy, and compensating defects. It is important to realize that the larger the energy gap, the higher the concentration of compensating point defects that is at equilibrium with the system, effectively transforming a semiconductor that was intentionally doped to an insulator. This realization is leading research efforts to develop novel approaches for point defect control that lead to efficient doping, after the achievement of high crystalline quality films. Otherwise, this technology may not reach its intended functionality and applicability.

As outlined in section 8.4, the growth and integration of high-quality ternary InGaN epilayers over a wide range of composition has many challenges to overcome. The successful integration of InGaN alloys with almost 30% indium lead to not only important light emitting device structures and promising photovoltaic solar cell structures, but also emerging new optoelectronics ranging structures for optical communications in the 1.3-1.5 μm range to structures cover the whole visible spectral range within one material system. The huge potential of InGaN based materials structures for envisioned energy saving- and energy generating devices provides sufficient incentives to expand research efforts towards new avenues and approaches to stabilize InGaN alloys over the entire composition range. Various concepts - from superatmospheric growth to off-equilibrium techniques such as rf-plasma assisted MOCVD - showed that alloys over the entire InGaN can be formed. The improvement of the material quality the their integration with highly dissimilar group III-nitride alloys will remain an ongoing research effort.

8.6 InGaN based Photoelectrochemical cells for hydrogen generation

PEC solar fuel cell structures use solar energy for driving chemical processes, in particular the reduction of water for hydrogen generation. Theoretically a semiconductor with band gap greater than 1.23 eV (due to losses and over-potential, experimentally 1.6 eV or greater is required) and conduction and valence band edges that straddle the electrochemical potentials for $H+/H_2$ and H_2O/O_2 respectively is required.[106] For thermodynamic stability against photodecomposition, the conduction and valence band edges must be more negative than the reduction decomposition potential (stable against cathodic decomposition) and more positive than oxidation decomposition potential (stable against anodic decomposition) respectively in water.[107] Very few semiconductors meet all these requirements. One of the favored semiconductors, TiO_2 meets the hydrogen generation requirements and is stable against cathodic decomposition and shows good corrosion resistance, but a large band gap results in very poor efficiency. A dual band gap configuration with two different semiconductors results in higher efficiencies. However stability and corrosion resistance when immersed remain as issues.

InGaN meets the requirements for hydrogen generation (up to 50% Indium Moses et al.[19].) as both photoanode and photocathode and has a highly tunable band gap (0.7 to 3.4 eV) and may be optimized for solar radiation for improved efficiency and photocurrent. **Figure 8.11:** shows a band diagram for n-InGaN near the semiconductor/electrolyte interface illustrating the alignment of the semiconductor bands with respect to the reduction/oxidation potentials. High corrosion

resistance and stability is expected due to a small lattice constant and strong bonding and InGaN has been shown to be resistant against wet etchants and stable in aqueous solutions.[108] Fujii et al.[109] have fabricated Si doped n- $In_xGa_{1-x}N$ (x=0.02 and x=0.09) PEC cells and have found increased photocurrents for $In_xGa_{1-x}N$ with an applied bias compared to GaN but with lower currents at zero bias (attributed to conduction band edge potential reduction). However Li et al.[109] have reported Si doped n-$In_xGa_{1-x}N$ epilayers on GaN based PECs with increased photocurrent with x=0.4 as compared to x=0.2 for all biases. Photogenerated holes are considered to be strong oxidizers and could oxidize the semiconductor itself[110] and Theuwis et al.[111] have reported photo-anodic etching of n-type InGaN under illumination with forward bias. It has been reported that p-type semiconductors have characteristics of hydrogen production at the surface[110] and exhibit resistance against oxidation due to electron accumulation under illumination.[112] Hence p-type InGaN presents a high efficiency candidate for hydrogen generation. Aryal et al.[113] have observed hydrogen generation with p-type Mg doped $In_xGa_{1-x}N$($0<x<0.22$) electrodes with additional bias with higher conversion efficiencies compared to p-GaN. Their stability in HBr solution was verified. Hwang et al.[114] have fabricated $In_{0.1}Ga_{0.9}N$ nanowires on Si wires for improved photocatalytic activity through increased surface area and improved charge separation.

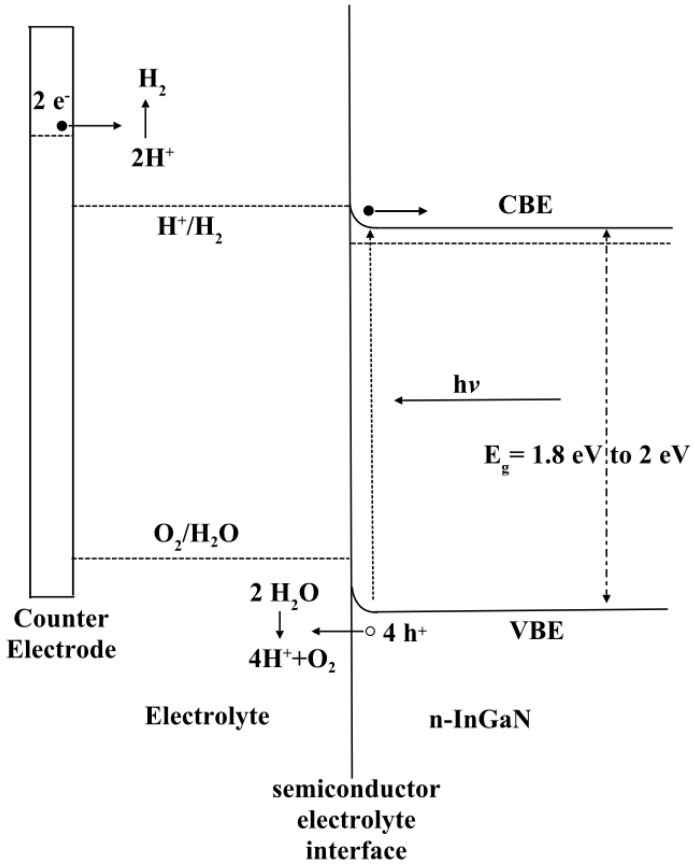

Figure 8.12:

Band diagram for n-InGaN near the electrolyte / semiconductor interface. The In-fraction is expected to be less than 50%.

8.7 Conclusion

We provided in this contribution a review of the physical properties of group III-nitrides - e.g. AlN, GaN, InN, and their ternary and quarternary alloys and discussed the present state and challenges in the materials growth, materials integration, and the physical materials properties improvements. As shown, group III-nitride compounds have a significant potential as semiconducting photoelectrode materials in PEC solar fuel cell structures. The band alignments in the ternary InGaN and InAlN alloy systems can be engineered over a wide energy range, providing for suitable energetic alignments of the semiconductor bands with the HOMO and LUMO levels of catalysts and for efficient charge transfer. Recent advances in group III-nitride materials stabilization and materials quality are encouraging to proceed with their integration in PEC cells and the evaluation of such device structures. Further advances are needed in the stabilization of ternary, indium-rich InGaN and InAlN alloys and their integration into dissimilar group III-nitride alloys in order to take advantage of the full potential of the group III-nitride system,

Acknowledgement

ND acknowledges the support by AFOSR under award # FA9550-10-1-0097.

References

1. S. Strite and H. Morkoc, "GaN, AlN, and InN: A review," J. Vac. Sci. Technol. B **10**, pp.1237-1266 (1992).
2. O Ambacher, "Growth and applications of Group III-nitrides", J. Phys. D: Appl. Phys. **31** pp. 2653-2710 (1998).
3. C. Wood et al., "Wide bandgap semiconducting materials and device challenges," Naval Research Reviews **51**(1), p. 4-76 (1999).
4. I. Vurgaftman, J. R. Meyer and L. R. Ram-Mohan, "Band parameters for III–V compound semiconductors and their alloys", J. Appl. Phys. **89**, pp.5815 - 5875 (2001).
5. I. Vurgaftman and J.R. Meyer, "Band parameters for nitrogen-containing semiconductors", J. Appl. Phys. **94**, pp. 3675-3696 (2003).
6. V. Yu. Davydov and A. A. Klochikhin, "Electronic and Vibrational States in InN and $In_xGa_{1-x}N$ Solid Solutions," Semiconductors **38**(8), pp. 861-898 (2004).
7. Handbook of Nitride Semiconductors and Devices. Vol. 1; ed. Hadis Morkoc, WILEY-VCH Verlag GmbH & Co. KGaA, Weinheim, ISBN: 978-3-527-40837-5; pp. 1-1311 (2008).
8. F. K. Yam and Z. Hassan, "InGaN: An overview of the growth kinetics, physical properties and emission mechanisms," Superlattices Microstruct. **43**(1) pp.1-23 (2008).
9. S. Chattopadhyay, A. Ganguly, K.-H. Chen and L.-C. Chen, "One-Dimensional Group III-Nitrides: Growth, Properties, and Applications in Nanosensing and Nano-Optoelectronics," Critical Reviews in Solid State and Materials Sciences **34**, pp.224-279 (2009).
10. J. Wu, "When group-III nitrides go infrared: New properties and perspectives," J. Appl. Phys. **106**(1) pp. 011101-28 (2009).
11. P. G. Moses, M. Miao, Q. Yan and C. G. Van de Walle, "Hybrid functional investigations of band gaps and band alignments for AlN, GaN, InN, and InGaN," J. Chem. Phys. **134,** p. 084703 (2011).
12. K. M. Yu, Z. Liliental-Weber, W. Walukiewicz, W. Shan, J. W. Ager, III, S. X. Li, R. E. Jones, E. E. Haller, Hai Lu, and William J. Schaff, "On the crystalline structure, stoichiometry and band gap of InN thin films," Appl. Phys. Lett. **86**(7), pp.071910-2 (2005)
13. A. Belabbes, J. Furthmüller and F. Bechstedt, "Electronic properties of polar and nonpolar InN surfaces: A quasiparticle picture," Phys. Rev. B **84**(20), 205304 (2011).
14. L. C. de Carvalho, A. Schleife, J. Furthmüller and F. Bechstedt, "Distribution of cations in wurtzitic $In_xGa_{1-x}N$ and $In_xAl_{1-x}N$ alloys: Consequences for energetics and quasiparticle electronic structures," Phys. Rev. B **85**(11), p.115121 (2012).
15. M. Łopuszyński and J. A. Majewski, "Ordering in ternary nitride semiconducting alloys," Phys. Rev. B **85**(3), pp.035211-25 (2012).
16. I. Gorczyca, S. P. Łepkowski, T. Suski, N. E. Christensen and A. Svane, "Influence of indium clustering on the band structure of semiconducting ternary and quaternary nitride alloys," Phys. Rev. B **80** (7), p.075202 (2009).
17. W. Paszkowicz, S. Podsiadło and R. Minikayev, "Rietveld-refinement study of aluminium and gallium nitrides," J. Alloys Compd. **382**(1–2), pp.100-106 (2004).
18. E. Sakalauskas, Ö. Tuna, A. Kraus, H. Bremers, U. Rossow, C. Giesen, M. Heuken, A. Hangleiter, G. Gobsch and R. Goldhahn, "Dielectric function and bowing parameters of InGaN alloys," Phys. Stat. Solidi (b) **249**(3), pp.485-488 (2012).

19. P. G. Moses and C. G. Van de Walle, "Band bowing and band alignment in InGaN alloys," Appl. Phys. Lett. **96**(2), pp.021908-3 (2010).

20. G. Cosendey, J.-F. Carlin, N. A. K. Kaufmann, R. Butte and N. Grandjean, "Strain compensation in AlInN/GaN multilayers on GaN substrates: Application to the realization of defect-free Bragg reflectors," Appl. Phys. Lett. **98**(18), pp.181111-3 (2011).

21. C. Kruse, H. Dartsch, T. Aschenbrenner, S. Figge and D. Hommel, "Growth and characterization of nitride-based distributed Bragg reflectors," Phys. Stat. Solidi (b) **248**(8), pp.1748-1755 (2011).

22. J. Xie, X. Ni, M. Wu, J. H. Leach, U. Ozgur and H. Morkoc, "High electron mobility in nearly lattice-matched AlInN/AlN/GaN heterostructure field effect transistors," Appl. Phys. Lett. **91**(13), pp.132116-3 (2007).

23. R. R. Pela, C. Caetano, M. Marques, L. G. Ferreira, J. Furthmuller, and L. K. Teles, "Accurate band gaps of AlGaN, InGaN, and AlInN alloys calculations based on LDA-1/2 approach," Applied Physics Letters **98**(15), 151907-151903 (2011).

24. L. G. Ferreira, M. Marques and L. K. Teles, "Approximation to density functional theory for the calculation of band gaps of semiconductors," Phys. Rev. B **78**(12) p.125116 (2008).

25. P. D. C. King, T. D. Veal, P. H. Jefferson, C. F. McConville, T. Wang, P. J. Parbrook, H. Lu and W. J. Schaff, "Valence band offset of InN/AlN heterojunctions measured by x-ray photoelectron spectroscopy," Appl. Phys. Let. **90**(13), pp.132105-3 (2007).

26. T. Makimoto, K. Kumarkura, T. Nishida and N. Kobayashi, , "Valence-band discontinuities between InGaN and GaN evaluated by capacitance-voltage characteristics of p-InGaN/n-GaN diodes," J. Electron. Mater. **31**(4), 313-315 (2002).

27. P. D. C. King, T. D. Veal, C. E. Kendrick, L. R. Bailey, S. M. Durbin and C. F. McConville, "InN/GaN valence band offset: High-resolution x-ray photoemission spectroscopy measurements," Phys. Rev. B **78**(3), p. 033308 (2008).

28. C.-L. Wu, H.-M. Lee, C.-T. Kuo, C.-H. Chen and S. Gwo, "Cross-sectional scanning photoelectron microscopy and spectroscopy of wurtzite InN/GaN heterojunction: Measurement of ``intrinsic'' band lineup," Appl. Phys. Lett. **92**(16), pp.162106-162103 (2008).

29. M. Akazawa, B. Gao, T. Hashizume, M. Hiroki, S. Yamahata and N. Shigekawa, "Measurement of valence-band offsets of InAlN/GaN heterostructures grown by metal-organic vapor phase epitaxy," J. Appl. Phys. **109**(1), pp.013703-8 (2011).

30. W. G. Breiland, M. E. Coltrin, J. R. Creighton, H. Q. Hou, H. K. Moffat and J. Y. Tsao, "Organometallic vapor phase epitaxy (OMVPE)," Mat. Sci. Eng. R **24**(6), pp.241-274 (1999).

31. R. F. Davis, S. M. Bishop, S. Mita, R. Collazo, Z. J. Reitmeier and Z. Sitar, "Epitaxial growth of gallium nitride," Aip Conf Proc **916**, pp.520-540 (2007).

32. K. Motoki, T. Okahisa, S. Nakahata, N. Matsumoto, H. Kimura, H. Kasai, K. Takemoto, K. Uematsu, M. Ueno, Y. Kumagai, A. Koukitu and H. Seki, "Growth and characterization of freestanding GaN substrates," J. Cryst. Growth **237-239**, pp.912-921 (2002).

33. P. Kempisty, B. Łucznik, B. Pastuszka, I. Grzegory, M. Boćkowski, S. Krukowski and S. Porowski, "CFD and reaction computational analysis of the growth of GaN by HVPE method," J. Cryst. Growth **296**, pp.31-42 (2006).

34. K. Hanaoka, H. Murakami, Y. Kumagai and A. Koukitu, "Thermodynamic analysis on HVPE growth of InGaN ternary alloy," J. Cryst. Growth **318**, pp.441-445 (2011).

35. Y. Kumagai, K. Takemoto, A. Koukitu and H. Seki, "Thermodynamics on halide vapor-phase epitaxy of InN using InCl and InCl3," J. Crys. Growth **222**, pp.118-124 (2001).

36. Y. Kumagai, J. Kikuchi, Y. Nishizawa, H. Murakami and A. Koukitu, "Hydride vapor phase epitaxy of InN by the formation of InCl3 using In metal and Cl2," J. Cryst. Growth, **300**(1) pp.57-61 (2007).

37. H. Lu, W.J. Schaff, J. Hwang, H. Wu, W.y Yeo, A. Pharkya, and L. F. Eastman, "Improvement on epitaxial grown of InN by migration enhanced epitaxy," Appl. Phys. Let. **77**(16) pp.2548-2550 (2000).

38. M. Higashiwaki and T. Matsui, "Plasma-assisted MBE growth of InN films and InAlN/InN heterostructures," J. Cryst. Growth **251**, pp.494-498 (2003).

39. K. S. A. Butcher, A. J. Fernandes, P. P.-T. Chen, M. Wintrebert-Fouquet, H. Timmers, S. K. Shrestha, h. Hirshy, R. M. Perks, and B. F. Usher, "The nature of nitrogen related point defects in common forms of InN," J. Appl. Phys. **101**, pp.123702-13 (2007).

40. S. Valdueza-Felip, J. Ibáñez, E. Monroy, M. González-Herráez, L. Artús and F. B. Naranjo, "Improvement of InN layers deposited on Si(111) by RF sputtering using a low-growth-rate InN buffer layer," Thin Solid Films **520**, pp.2805-2809 (2012).

41. K. J. Bachmann, H. T. Banks, C. Hopfner, G. M. Kepler, S. LeSure, S. D. McCall and J. S. Scroggs, "Optimal design of a high pressure organometallic chemical vapor deposition reactor," Mathematical and Computer Modelling **29**(8) pp. 65-80. (1999).

42. "Indium-nitride growth by HPCVD: Real-time and ex-situ characterization," N. Dietz, book chapter 6 in "III-Nitrides Semiconductor Materials", ed. Z.C. Feng, Imperial College Press, ISBN 1-86094-636-4, pp. 203-235 (2006).

43. M. Buegler, S. Gamage, R. Atalay, J. Wang, M. K. I. Senevirathna, R. Kirste, T. Xu, M. Jamil, I. Ferguson, J. Tweedie, R. Collazo, A. Hoffmann, Z. Sitar, and N. Dietz, "Growth temperature and growth rate dependency on reactor pressure for InN epilayers grown by HPCVD," Phys. Stat. Sol. (c) **8** pp. 2059-2062 (2011).

44. A. Dadgar, P. Veit, F. Schulze, J. Bläsing, A. Krtschil, H. Witte, A. Diez, T. Hempel, J. Christen, R. Clos and A. Krost, "MOVPE growth of GaN on Si – Substrates and strain," Thin Solid Films **515**(10), 4356-4361 (2007).

45. D. Ehrentraut and Z. Sitar, "Advances in Bulk Crystal Growth of AlN and GaN," MRS Bulletin **34**, pp.259-265 (2009).

46. Y. Kobayashi, K. Kumakura, T. Akasaka and T. Makimoto, "Layered boron nitride as a release layer for mechanical transfer of GaN-based devices," Nature **484**, pp.223-227 (2012).

47. R. Dalmau, B. Moody, R. Schlesser, S. Mita, J. Xie, M. Feneberg, B. Neuschl, K. Thonke, R. Collazo, A. Rice, J. Tweedie and Z. Sitar, "Growth and Characterization of AlN and AlGaN Epitaxial Films on AlN Single Crystal Substrates," J. Electrochem. Soc. **158**, H530 (2011).

48. J. R. Grandusky, S. R. Gibb, M. C. Mendrick, C. Moe, M. Wraback and L. J. Schowalter, "High Output Power from 260nm Pseudomorphic Ultraviolet Light-Emitting Diodes with Improved Thermal Performance," Applied Physics Express **4**, pp.082101-3 (2011).

49. M. Kneissel, T. Kolbe, C. Chua, V. Kueller, N. Lobo, J. Stellmach, A. Knauer, H. Rodriguez, S. Einfeldt, Z. Yang, N. M. Johnson and M. Weyers, "Advances in group III-nitride-based deep UV light-emitting diode technology," Sem. Sci. Technol. **26**, 014036 (2011).

50. T. Wunderer, C. L. Chua, Z. H. Yang, J. E. Northrup, N. M. Johnson, G. A. Garrett, H. G. Shen and M. Wraback, "Pseudomorphically Grown Ultraviolet C Photopumped Lasers on Bulk AlN Substrates," Appl. Phys. Express **4**, pp.092101-3 (2011).

51. F. Bernardini, V. Fiorentini and D. Vanderbilt, "Spontaneous polarization and piezoelectric constants of III-V nitrides," Physical Review B **56**(16), 10024-10027 (1997).

52. C. J. Sun, P. Kung, A. Saxler, H. Ohsato, E. Bigan, M. Razeghi and D. K. Gaskill, "Thermal stability of GaN thin films grown on (0001) Al2O3, (011-bar 2) Al2O3 and (0001)Si 6H-SiC substrates," J. Appl. Phys. **76**, 236 (1994).

53. S. Mita, R. Collazo and Z. Sitar, "Fabrication of a GaN lateral polarity junction by metalorganic chemical vapor deposition," J. Cryst. Growth **311**, pp.3044-3048 (2009).

54. W. K. Burton, N. Cabrera and F. C. Frank, "The Growth of Crystals and the Equilibrium Structure of Their Surfaces," Philos Tr R Soc S-A **243**(866), pp.299-358 (1951).

55. S. Mita, R. Collazo, A. Rice, R. F. Dalmau and Z. Sitar, "Influence of gallium supersaturation on the properties of GaN grown by metalorganic chemical vapor deposition," J. Appl. Phys. **104**, 013521 (2008).

56. T. Paskova and K. R. Evans, "GaN Substrates-Progress, Status, and Prospects," IEEE J. Sel. Top. Quant. **15**(4), pp.1041-1052 (2009).

57. P. Lu, R. Collazo, R.F. Dalmau, G. Durkaya, N. Dietz, B. Raghothamachar, M. Dudley, Z. Sitar, "Seeded growth of AlN bulk crystals in m- and c-orientation," J. Cryst. Growth, **312**(1) pp. 58-63 (2009).

58. C. Herring, "Some Theorems on the Free Energies of Crystal Surfaces," Phys. Rev. **82**, pp.87–93 (1951).

59. A. Rice, R. Collazo, J. Tweedie, R. Dalmau, S. Mita, J. Xie and Z. Sitar, "Surface preparation and homoepitaxial deposition of AlN on (0001)-oriented AlN substrates by metalorganic chemical vapor deposition," J. Appl. Phys. **108**, 043510 (2010).

60. C. I. Wu, A. Kahn, E. S. Hellman and D. N. E. Buchanan, "Electron affinity at aluminum nitride surfaces," Appl. Phys. Lett. **73**, 1346 (1998).

61. J. W. Ager, N. Miller, R. E. Jones, K. M. Yu, J. Wu, W. J. Schaff and W. Walukiewicz, "Mg-doped InN and InGaN - Photoluminescence, capacitance-voltage and thermopower measurements," Phys. Stat. Sol. B **245**, pp.873–877 (2008).

62. G. B. Stringfellow, "Organometallic Vapor-Phase Epitaxy: Theory and Practice," ISBN: 0126738424, Academic Press, Boston, (1998).

63. Hildebrand J.H., "Solubility. XII. Regular Solutions", J. Am. Chem. Soc. **51**, pp. 66-80, 1929

64. I. H. Ho and G. B. Stringfellow, "Solid phase immiscibility in GaInN," Appl. Phys. Lett. **69**, 2701 (1996).

65. Y. A. Xi, K. X. Chen, F. W. Mont, J. K. Kim, W. Lee, E. F. Schubert, W. Liu, X. Li, and J. A. Smart, Appl. Phys. Lett. **90**, 051104 (2007).

66. A. Rice, R. Collazo, J. Tweedie, J. Xie, S. Mita and Z. Sitar, "Linear dependency of Al-mole fraction with group-III precursor flows in AlxGa1-xN (0 <= x <= 1) deposition by LP OMVPE," J. Crysy. Growth **312**, pp.1321-1324 (2010).

67. C. G. Van de Walle and J. Neugebauer, "First-principles calculations for defects and impurities: Applications to III-nitrides," J. Appl. Phys. **95**, pp.3851-3879 (2004).

68. K. Zhu, M. L. Nakarmi, K. H. Kim, J. Y. Lin and H. X. Jiang, "Silicon doping dependence of highly conductive n-type $Al_{0.7}Ga_{0.3}N$," Appl. Phys. Let. **85,** pp.4669-4671 (2004).

69. C. Stampfl and C. G. Van de Walle, "Theoretical investigation of native defects, impurities, and complexes in aluminum nitride," Phys. Rev. B **65**, pp.155212-10 (2002).

70. C. G. Van de Walle, "DX-center formation in wurtzite and zinc-blende $Al_xGa_{1-x}N$," Phys. Rev. B **57**, R2033-R2036 (1998).

71. R. Zeisel, M. W. Bayerl, S. T. B. Goennenwein, R. Dimitrov, O. Ambacher, M. S. Brandt and M. Stutzmann, "DX-behavior of Si in AlN," Phys. Rev. B **61**, pp.R16283-R16286 (2000).

72. M. L. Nakarmi, N. Nepal, J. Y. Lin and H. X. Jiang, "Unintentionally doped n-type Al0.67Ga0.33N epilayers," Appl. Phys. Lett. **86**, p.261902 (2005).

73. J. Neugebauer and C. G. Vandewalle, "Atomic Geometry and Electronic-Structure of Native Defects in GaN," Phys. Rev. B **50,** pp.8067–8070 (1994).

74. N. Nepal, M. L. Nakarmi, J. Y. Lin and H. X. Jiang, "Photoluminescence studies of impurity transitions in AlGaN alloys," Appl. Phys. Lett. **89**, pp.092107-3 (2006).

75. J. Slotte, F. Tuomisto, K. Saarinen, C. G. Moe, S. Keller and S. P. DenBaars, "Influence of silicon doping on vacancies and optical properties of $Al_xGa_{1-x}N$ thin films," Appl. Phys. Lett. **90**, pp.151908-3 (2007)

76. T. Tanaka, A. Watanabe, H. Amano, Y. Kobayashi, I. Akasaki, S. Yamazaki and M. Koike, "P-Type Conduction in Mg-Doped Gan and Al0.08ga0.92n Grown by Metalorganic Vapor-Phase Epitaxy," Appl. Phys. Let. **65**, pp.593-594 (1994).

77. C. G. Van de Walle, C. Stampfl, J. Neugebauer, M. D. McCluskey and N. M. Johnson, "Doping of AlGaN alloys," Mrs Internet JNSR **4**, pp.G10.14 (1999).

78. S. Nakamura, T. Mukai and M. Senoh, "Candela-class high-brightness InGaN/AlGaN double-heterostructure blue-light-emitting diodes," Appl. Phys. Lett. **64**(13), pp. 1687-3 (1994);

79. S. Nakamura, M. Senoh, S.-i. Nagahama, N. Iwasa, T. Yamada, T. Matsushita, H. Kiyoku and Y. Sugimoto, "InGaN-Based Multi-Quantum-Well-Structure Laser Diodes," Jpn. J. Appl. Phys. **35** pp. L74-L76 (1996).

80. R. M. Farrell, E. C. Young, F. Wu, S. P. DenBaars and J. S. Speck, "Materials and growth issues for high-performance nonpolar and semipolar light-emitting devices," Semicond. Sci. Technol. **27** pp.024001-15 (2012).

81. J. MacChesney, P.M. Bridenbaugh, and P.B. O'Connor, "Thermal stability of indium nitride at elevated temperatures and nitrogen pressures," Mater. Res. Bull. **5** pp. 783-792 (1970).

82. G. B. Stringfellow, "Microstructures produced during the epitaxial growth of InGaN alloys," J. Cryst. Growth **312**(6), pp.735-749 (2010).

83. V. Vasil'ev and J. Gachon, "Thermodynamic properties of III–V compounds," Inorganic Materials **42**(11), pp.1176-1187 (2006).

84. Md. Tanvir Hasan, Ashraful G. Bhuiyan and Akio Yamamoto, "Two dimensional electron gas in InN-based heterostructures: Effects of spontaneous and piezoelectric polarization," Solid-State Electronics **52**(1) pp. 134-139 (2008).

85. T. P. Bartel and C. Kisielowski, "A quantitative procedure to probe for compositional inhomogeneities in InxGa1-xN alloys," Ultramicroscopy **108**, 1420 (2008).

86. M. G. Ganchenkova, V. A. Borodin, K. Laaksonen, and R. M. Nieminen, "Modeling the compositional instability in wurtzite $Ga_{1-x}In_xN$," Phys. Rev. B **77**, 075207 (2008).

87. J. Zheng and J. Kang, "Theoretical study of phase separation in wurtzite InGaN," Materials Science in Semiconductor Processing **9**, 341 (2006).

88. M.-K. Chen, Y.-C. Cheng, J.-Y. Chen, C.-M. Wu, C. C. Yang, K.-J. Ma, J.-R. Yang and A. Rosenauer, "Effects of silicon doping on the nanostructures of InGaN/GaN quantum wells," J. Cryst. Growth **279**(1-2) pp.55-64 (2005).

89. S. Yu. Karpov, "Suppression of phase separation in InGaN due to elastic strain," MRS Internet J. Nitride Semicond. Res. **3,** 16(1998).

90. N. A. El-Masry, E. L. Piner, S. X. Liu, and S. M. Bedair, "Phase separation in InGaN grown by metalorganic chemical vapor deposition," Appl. Phys. Let. **72**, pp.40-42 (1998).

91. I. Ho and G.B. Stringfellow, "Solid phase immiscibility in GaInN," Appl. Phys. Lett. **69** p. 2701-03 (1996).

92. G. Stringfellow, "Spinodal decomposition and clustering in III/V alloys," Journal of Electronic Materials **11**(5), pp.903-918 (1982).

93. M. Alevli, G. Durkaya, W. Fenwick, A. Weerasekara, V. Woods, I. Ferguson, A.G.U. Perera and N. Dietz, "The characterization of InN layers grown by high-pressure chemical vapor deposition," Appl. Phys. Lett. **89**, pp. 112119 (2006).

94. N. Dietz, M. Alevli, R. Atalay, G. Durkaya, R. Collazo, J. Tweedie, S. Mita, and Z. Sitar, "The influence of substrate polarity on the structural quality of InN layers grown by high-pressure chemical vapor deposition,", Appl. Phys. Lett. **92**(4) pp. 041911-3 (2008).

95. G. Durkaya, M. Alevli, M. Buegler, R. Atalay, S. Gamage,M. Kaiser, R. Kirste, A. Hoffmann, M. Jamil, I. Ferguson and N. Dietz, "Growth temperature - phase stability relation in In1-xGaxN epilayers grown by high-pressure CVD," Mater. Res. Soc. Symp. Proc. **1202**, MRS Symposium I: III-Nitride Materials for Sensing, Energy Conversion, and Controlled Light-Matter Interactions, paper# 1202-I5.21, pp.1-6 (2010).

96. R. Kirste, M. R. Wagner, J. H. Schulze, A. Strittmatter, R. Collazo, Z. Sitar, M. Alevli, N. Dietz and A. Hoffmann, "Optical properties of InN grown on templates with controlled surface polarities," Phys. Stat. Solidi A **207** pp. 2351–2354 (2010).

97. M. Buegler, S. Gamage, R. Atalay, J. Wang, I. Senevirathna, R. Kirste, T. Xu, M. Jamil, I. Ferguson, J. Tweedie, R. Collazo, A. Hoffmann, Z. Sitar, and N. Dietz, "Reactor pressure - growth temperature relation for InN epilayers grown by high-pressure CVD," Proc. of SPIE Vol. **7784**, doi: 10.1117/12.860952, paper# 77840F-1-7 (2010).

98. D.J. As, "Cubic group-III nitride-based nanostructures--basics and applications in optoelectronics," Journal Microelectronics 40(2), pp. 204-209 (2009).

99. S. Choi, H. J. Kim, J.-H. Ryou, and R. D. Dupuis, "Digitally alloyed modulated precursor flow epitaxial growth of $Al_xGa_{1-x}N$ layers with AlN and $Al_yGa_{1-y}N$ monolayers," J. Cryst. Growth **311**(12) pp. 3252-3256 (2009).

100. J. Grandal, J. Pereiro, A. Bengoechea-Encabo, S. Fernandez-Garrido, M. A. Sanchez-Garcia, E. Munoz, E. Calleja, E. Luna, and A. Trampert, "InN/InGaN multiple quantum wells emitting at 1.5 mu m grown by molecular beam epitaxy," Appl. Phys. Lett. **98**, 061901 (2011), DOI:10.1063/1.3552195

101. V. Lebedev et al., "Effect of island coalescence on structural and electrical properties of InN thin films," J. Cryst. Growth **300**, pp. 50-56 (2007).

102. Akihiko Yoshikawa, Songbek Che, Yoshihiro Ishitani, Xinqiang Wang, "Advances in InN epitaxy and its material control by MBE towards novel InN-based QWs," Journal of Crystal Growth **311**(7) pp.2073-2079 (2009).

103. T. Takeuchi, S. Sota, M. Katsuragawa, M. Komori, H. Takeuchi, H. Amano and I. Akasaki, "Quantum-Confined Stark Effect due to Piezoelectric Fields in GaInN Strained Quantum Wells," Jpn. J. Appl. Phys. **36**, L382-L385 (1997).

104. S. Chichibu, T. Azuhata, T. Sota, S. Nakamura, "Spontaneous emission of localized excitons in InGaN single and multiquantum well structures," Appl. Phys. Lett. **69**(27) pp.4188-4190 (1996).

105. S. Chichibu et al, "Origin of defect-insensitive emission probability in In-containing (Al,In,Ga)N alloy semiconductors," Nature Materials **5**, pp. 810-816 (2006)

106. M.G. Walter, E.L. Warren, J. R. McKone, S.W. Boettcher, Q.M., Elizabeth A. Santori, and N. S. Lewis, "Solar Water Splitting Cells," Chem. Rev. **110**(11), pp. 6446-6473 (2010).

107. H. Gerischer, "On the stability of semiconductor electrodes against photodecomposition," J. Electroanal. Chem. **82** (1–2), pp.133-143 (1977).

108. C. B. Vartuli, S. J. Pearton, C. R. Abernathy, J. D. MacKenzie, F. Ren, J. C. Zolper, and R. J. Shul, "Wet chemical etching survey of III-nitrides," Solid-State Elect. **41**(12), pp.1947-1951 (1997).

109. J. Li, J. Y. Lin, and H. X. Jiang, "Direct hydrogen gas generation by using InGaN epilayers as working electrodes," Appl. Phys. Lett. **93**(16), pp.162107-162103 (2008).

110. K. Fujii, K. Kusakabe, and K. Ohkawa, "Photoelectrochemical Properties of InGaN for H_2 Generation from Aqueous Water," Jpn. J. Appl. Phys. **44** pp.7433-7435 (2005).

111. A. Theuwis, K. Strubbe, L. M. Depestel, and W. P. Gomes, "A Photoelectrochemical Study of $In_xGa_{1-x}N$ Films," J. Electrochem. Soc. **149**(5) pp.E173-E178 (2002).

112. K. Fujii, K. Ohkawa, "Photoelectrochemical Properties of p-Type GaN in Comparison with n-Type GaN," .Jpn. J. Appl. Phys. **44** p.L909 (2005)

113. K. Aryal, B. N. Pantha, J. Li, J. Y. Lin, H. X. Jiang, Hydrogen generation by solar water splitting using p-InGaN photoelectrochemical cells," Appl. Phys. Lett. **96**, p.052110 (2010).

114. Y. J. Hwang, C. H. Wu, C. Hahn, H. E. Jeong, and P. Yang, "Si/InGaN core/shell hierarchical nanowire arrays and their photoelectrochemical properties," Nano Letters **12**(3), pp.1678-1682 (2012).